Results in Physics 10 (2018) 731–737

Contents lists available at ScienceDirect

Results in Physics

journal homepage: www.elsevier.com/locate/rinp

Effect of alumina nano-particle size and weight content on the corrosion resistance of AA1070 aluminum in chloride/sulphate solution

Roland Tolulope Loto*, Phillip Babalola

Department of Mechanical Engineering, Covenant University, Ota, Ogun State, Nigeria

ARTICLE INFO

Keywords:
Pitting
Corrosion
Alumina
Aluminum
Composite

ABSTRACT

The effect of specific alumina (Al_2O_3) nano-particle sizes (500 nm and 80 nm) and weight content (5% and 10%) on the electrochemical characteristics and corrosion resistance of AA1070 monolithic aluminum alloy (1070AL) in 0.1 M H_2SO_4, 1.78% NaCl and 0.1 M H_2SO_4/1.78% NaCl solutions was evaluated by potentiodynamic polarization test, open circuit potential measurement and optical microscopy analysis. The composite specimens at 80 nm particle size generally had lower corrosion rates than their composite counterparts. Results showed the combined sulphate/chloride solution severely deteriorated the surface properties of 1070AL and the alumina aluminum matrix composites (1070AL/Al_2O_3) coupled with having the highest corrosion rate values. The extent of surface deterioration was relatively smaller for 1070AL/Al_2O_3 specimens. Corrosion pits and intergranular cracks were observed on the surface morphology of 1070AL and 1070AL/Al_2O_3 specimens in NaCl solution despite having the lowest corrosion rate values. Significant passivation behavior was observed the specimens during potential scanning despite their highly electronegative corrosion potentials. SO_4^{2-} anions in H_2SO_4 solution did not cause any significant change on morphology of the aluminum specimens with respect to the corrosion rate values being the second highest by comparison. 1070AL/Al_2O_3 at 80 nm and 10% weight content had the lowest corrosion rate among the composites which was comparable to 1070AL in 0.1 M H_2SO_4 and 1.78% NaCl solution.

Introduction

Aluminum matrix composites are a class of light weight high performance materials with extensive applications in military aerospace, automobile, space, biotechnology, semi-conductor, nuclear, sports and recreational industries. The composites such as silicon carbide, alumina, titanium oxide, boron carbide etc. are added within the aluminum substrate through specialized processes. They are usually non-metallic reinforcement particles which improves the thermal conductivity of the base metal in addition to excellent abrasion resistance, creep resistance, abrasion resistance and excellent stiffness and strength to weight ratio. Alumina is an inorganic ceramic compound and oxide of aluminum existing naturally as bauxite, corundum, etc. It is used as a desiccating agent, a catalyst, an adsorbent, in the production of dental cements and refractories. The exceptional properties of alumina such as very high hardness value even at very high temperatures, chemically inactive, strong wear resistance and high melting point. Alumina is responsible for the resistance of metallic aluminum to weathering and previous research has proven it to be highly resistant to corrosion in aqueous solutions enabling its application as a reactor material in the supercritical water oxidation process [1]. Ćurković et al. showed that the corrosion rate of alumina ceramics decreased in high molar concentrations of HCl and H_2SO_4 solutions [2]. The dissolution rate of a variety of alumina-based ceramics in azeotropic aqueous hydrofluoric acid at 200 °C showed corrosion occurred at the grain boundaries [3]. Studies by Lazar et al. [4] on the corrosion of 304L stainless steel coated by alumina through metal–organic chemical vapor deposition in a dilute NaCl showed that the alumina at specific coating thickness proves to be highly corrosion resistant. Alaneme and Bodunrin [5] studied the influence of variation of volume percent and solution heat treatment of alumina on the corrosion resistance of 6063Al composites and base metal. Alumina is more stable, inert with higher temperature resistance than silicon carbide, the most applied matrix composite [6–9]. In automobile industry aluminum matrix composites with alumina has substituted cast iron components [10]. However, the work of Aylor and Taylor showed that localized corrosion occurred at the composite/matrix interface suggesting that the corrosion resistance of the matrix composites is subjective [11]. Research on the influence of reinforcement additives on the corrosion of aluminum matrix composites continues and is still the subject of intense study [12–14]. This

* Corresponding author.
E-mail address: tolu.loto@gmail.com (R.T. Loto).

https://doi.org/10.1016/j.rinp.2018.07.025
Received 17 May 2018; Received in revised form 16 July 2018; Accepted 18 July 2018
Available online 25 July 2018

Table 1
Percentage nominal composition of 1070AL.

Element Symbol	Fe	Si	Mn	Cu	Zn	Ti	Mg	Pb	Sn	Al
% Composition	0.232	0.078	0.000	0.0006	0.0016	0.006	0.0027	0.0012	0.007	99.66

Table 2
Designation of 1070AL and 1070AL/Al_2O_3 samples.

Sample	Aluminum %	Alumina %	Alumina particle size (nm)
A	100	–	0
B1	95	5	500
B2	90	10	
C1	95	5	80
C2	90	10	

investigation aims to study the effect of limited alumina particle size and content on the corrosion resistance 1070 aluminum alloy in H_2SO_4, NaCl and H_2SO_4/NaCl solution.

Materials and methods

Aluminium metal (1070AL) purchased from Aluminium Rolling Mills Company, Ota, Ogun State, Nigeria has nominal (wt%) composition shown in Table 1. Alumina nano-particles (Al_2O_3) of 500 nm and 80 nm were purchased from US Research Nano Materials Inc, Texas, USA. The particles were added to molten 1070AL at 650 °C in a tilting furnace to obtained aluminium alumina matrix composites (1070AL/Al_2O_3) at 5% and 10% weight content for 500 nm and 80 nm alumina particle sizes as shown in Table 2. The molten 1070AL/Al_2O_3 was stirred mechanically, cast into sand moulds and cooled for 24 h. 1070AL and 1070AL/Al_2O_3 were machined to obtained average surface areas of 1 cm^2 and metallographically prepared (after mounting in resin) with silicon carbide grinding papers (60, 120, 220, 600, 800 1000 grit) and diamond polishing paste (6 μm), before cleansing with distilled water and acetone for potentiodynamic polarization and open circuit potential measurement. Their Brinell hardness result is shown in Table 3. 0.1 M H_2SO_4 solution was prepared from analar grade of H_2SO_4 acid (98%, obtained from Sigma Aldrich) with distilled water. Analar grade NaCl obtained from Titan Biotech, India was prepared in volumetric concentration of 1.78% NaCl in distilled water, while 0.1 M H_2SO_4/1.78% NaCl was prepared from analar grade H_2SO_4 acid and NaCl.

Potentiodynamic polarization tests were performed 30 °C (ambient temperature) with Digi-Ivy 2311 electrochemical workstation. Graphical illustrations were obtained at scan rates of 0.0015 V/s between specific potentials for each electrolyte used. Corrosion current density, C_{cd} (A/cm^2) and corrosion potential, C_{pt} (V) values were determined from the graphical plots using Tafel extrapolation method. Corrosion rate, C_{RT} (mm/y) and inhibition efficiency, η (%) were obtained from the calculation below;

$$C_{RT}\frac{0.00327 \times C_{cd} \times E_q}{D} \quad (1)$$

D is the density in (g/cm^3); E_q is the alloy equivalent weight (g). 0.00327 is the constant for corrosion rate. Open circuit potential measurement (OCP) was performed at 0.05 V/s step potential for 3200 s to study the active-passive behavior of the alloy-solution system and their thermodynamic equilibrium with respect to time and the electrochemical action of the corrosive anions. Morphological representations of the corroded 1070AL and 1070AL/Al_2O_3 samples from optical microscopy were analysed after polarization test with Omax trinocular metallurgical microscope through the aid of ToupCam analytical software.

Table 3
Brinell hardness results.

Samples	Brinell hardness value
A	12.7
B1	13.6
B2	14.6
C1	14.6
C2	14.9

Results and discussion

Potentiodynamic polarization studies

The effect of Al_2O_3 nano-particles on the corrosion polarization behavior of 1070AL aluminum alloy in 0.1 M H_2SO_4, 1.78% NaCl and 0.1 M H_2SO_4/1.78% NaCl solution is shown from Fig. 1(a)–(c). Table 4 shows the polarization data obtained. Observation of the table shows the combined action of Cl^- and SO_4^{2-} anions in 0.1 M H_2SO_4/1.78% NaCl solution had the most destructive effect on 1070AL and 1070AL/Al_2O_3 aluminum composites due to their synergistic action during the redox electrochemical processes occurring at the interfacial layer of the metal alloys and matrix composites. Despite the relatively small size and strong electro-active nature of Cl^- anions, their influence on the deterioration of surface properties of the metal alloys in 1.78% NaCl solution was quite minimal from observation of the corrosion rate values. It is can clearly be established from the results that Cl^- anions has the least influence on the electrochemical properties of the aluminum alloy resulting into corrosion. However, the thermodynamic tendency of 1070AL and 1070AL/Al_2O_3 (sample A-C2) to corrode is much higher in 1.78% NaCl solution as observed from the corrosion potentials where the values tends to be more electronegative due to selective adsorption of Cl^- anions at the oxide layer. The lower corrosion rate combined with greater cathodic corrosion activity for the samples in 1.78% NaCl solution shows chloride-oxide complexes are likely being formed on the oxide surface at the expense of O_2 atoms due to O_2 reduction reactions. The anodic portion of the polarization plot in Fig. 1(b) shows visible passivation behavior which confirms the formation of chloride-oxide complexes leading to breakdown of the passive film after sufficient displacement of O2 at the transpassive region of the plot. The higher corrosion rate for the alloy and matrix composites in chloride-sulphate solution (0.1 M H_2SO_4/1.78% NaCl) shows Cl^-/SO_4^{2-} interaction interferes with the formation or repassivation of the passive film leading to severe deterioration of the surface properties and substrate of the alloy and matrix composites. Changes in anodic Tafel slope values in Table 4, signifies the likelihood of dominant anodic reactions. Sample A (1070AL) had the lowest corrosion rate in the electrolyte solutions studied due to its relatively homogeneous surface properties. The formation of Al_2O_3 on the metal surface is continuous with fewer flaws, impurities and less likely occurrence of galvanic effects among the intermetallic phases of the metal. 1070AL/Al_2O_3 (sample B1) at 500 nm Al_2O_3 composite size and 95% content displayed the highest corrosion rate in 0.1 M H_2SO_4 and 1.78% NaCl solutions. While 1070AL/Al_2O_3 (sample C1) at 80 nm Al_2O_3 composite size and 90% content showed the lowest corrosion rate in 0.1 M H_2SO_4 and 1.78% NaCl among the composite samples. The observation shows the likely relationship between Al_2O_3 particle size and content on the corrosion resistance of 1070AL/Al_2O_3. They affect the physiochemical stability of the oxide film in the presence of chloride and sulphate anions.

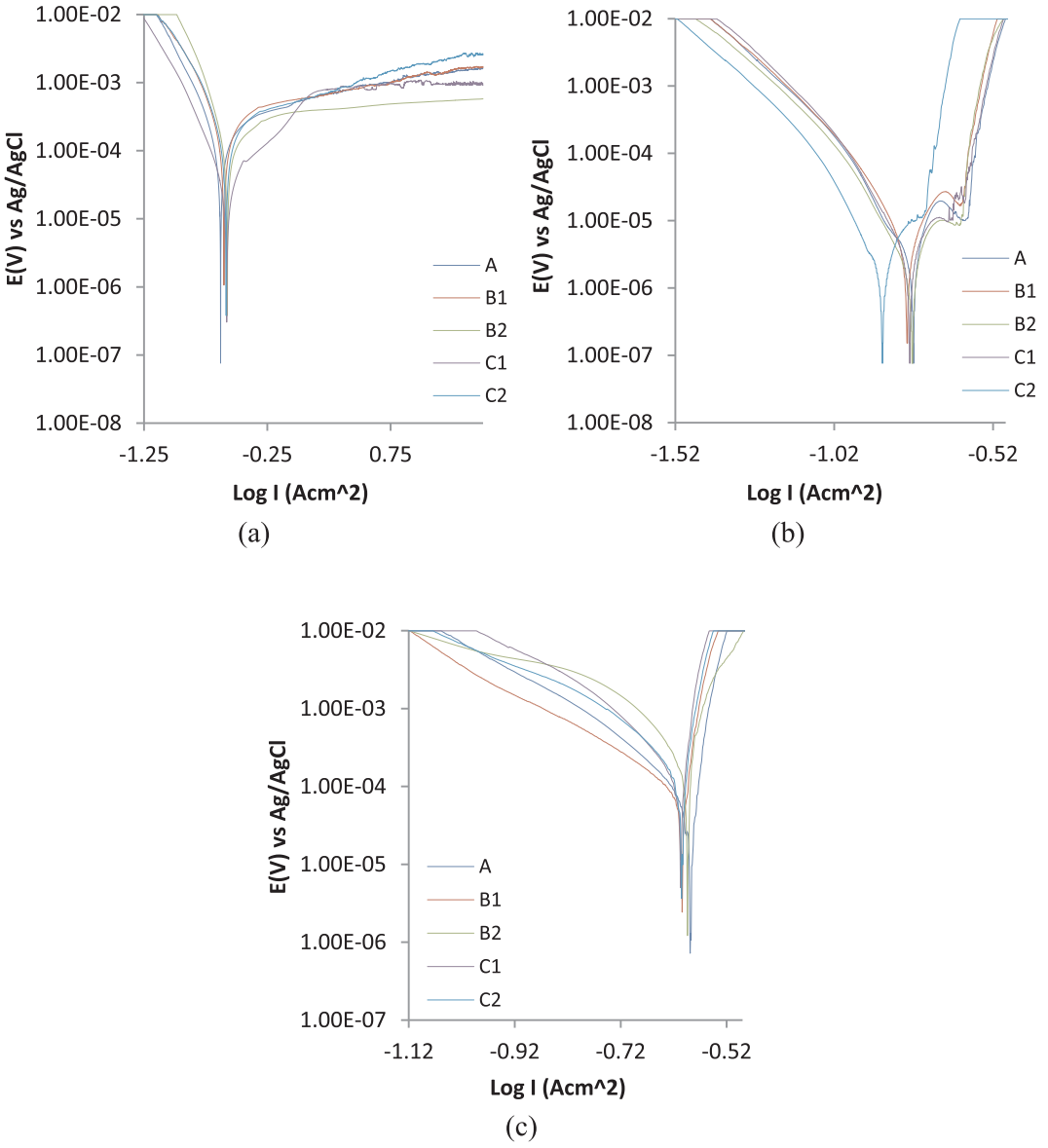

Fig. 1. Potentiodynamic polarization plots of 1070AL and 1070AL/Al_2O_3 (sample A-C2) in (a) 0.1 M H_2SO_4, (b) 1.78% NaCl and (c) 0.1 M H_2SO_4/1.78% NaCl solution.

The polarization plots depicting the active passive behavior of the aluminum metal alloy and composite samples [Fig. 1(a)–(c)] significantly contrast each other. Fig. 1(b) reveals the passivation characteristics of the samples studied. In the course of anodic polarization, the samples repassivated at specific current/potential values with respect to Al_2O_3 content and particle size. This phenomenon occurs after metastable pitting activity as shown by the decrease in the anodic slope of the plots. After which the plots showed the samples remained passive for at significant potential interval before breakdown due to pitting corrosion in the transpassive region of the curve. Beyond the transpassive region, a sharp increase of the anodic plots occurs, signifying unrestricted anodic dissolution of the samples. This is basically the reason why the corrosion rate values of the samples in 1.78% NaCl is relatively low. The major corrosion reactions taking place are localized while the remaining entire large surface areas of the samples are stable. Fig. 1(c) shows active behavior of the anodic-cathodic polarization plots due to instantaneous destruction of the protective oxide of the aluminum samples; hence no passivation of the samples occurred. The decreased anodic slope of Fig. 1(a) shows the aluminum samples gradually deteriorated during potential scanning.

Open circuit potential measurement (OCP)

The thermodynamic tendency of sample A, B1 and C1 to corrode in 0.1 M H_2SO_4, 1.78% NaCl and 0.1 M H_2SO_4/1.78% NaCl solutions are shown from Fig. 2(a)–(c). Variation of OCP values to exposure time significantly contrasts each other due to differences in metal-anion interaction. Observation of Fig. 2(a) shows visible decrease in OCP from −0.547 V, −0.507 V and −0.550 V (sample A, B1 and C1) at 0 s to −0.670 V, −0.627 V and −0.681 V at 250 s. This phenomenon is related instantaneous destruction of the protective oxide due to the electrochemical action of SO_4^{2-} anions in solution. However, sample B1 proves to be more thermodynamically stable than others with the least tendency to corrode at this point in time with an OCP value of

Table 4
Potentiodynamic polarization plots of 1070AL and 1070AL/Al_2O_3 (sample A-C2) in 0.1 M H_2SO_4, 1.78% NaCl and 0.1 M H_2SO_4/1.78% NaCl solution.

0.1 M H_2SO_4							
Alumina Content (%)	**Corrosion Rate (mm/y)**	**Corrosion Current (A)**	**Corrosion Current Density (A/cm^2)**	**Corrosion Potential (V)**	**Polarization Resistance, R_p (Ω)**	**Cathodic Tafel Slope, B_c (V/dec)**	**Anodic Tafel Slope, B_c (V/dec)**
A	0.523	4.82E-05	4.82E-05	−0.629	532.7	−7.394	4.807
B1	0.717	6.61E-05	6.61E-05	−0.602	388.9	−7.204	4.715
B2	0.631	5.82E-05	5.82E−05	−0.574	465.9	−7.538	3.972
C1	0.679	6.26E-05	6.26E-05	−0.579	410.5	−7.164	4.748
C2	0.618	5.69E-05	5.69E-05	−0.584	451.3	−7.346	4.800
1.78% NaCl							
Alumina Content (%)	**Corrosion Rate (mm/y)**	**Corrosion Current (A)**	**Corrosion Current Density (A/cm^2)**	**Corrosion Potential (V)**	**Polarization Resistance, R_p (Ω)**	**Cathodic Tafel Slope, B_c (V/dec)**	**Anodic Tafel Slope, B_c (V/dec)**
A	0.024	2.20E-06	2.20E-06	−0.770	613.30	−6.191	3.023
B1	0.045	4.14E-06	4.14E-06	−0.789	553.80	−8.966	5.482
B2	0.035	3.25E-06	3.25E-06	−0.780	790.70	−4.661	5.460
C1	0.038	3.47E-06	3.47E-06	−0.782	741.50	−8.651	3.417
C2	0.029	2.67E-06	2.67E-06	−0.768	963.30	−10.350	5.460
0.1 M H_2SO_4/1.78% NaCl							
Alumina Content (%)	**Corrosion Rate (mm/y)**	**Corrosion Current (A)**	**Corrosion Current Density (A/cm^2)**	**Corrosion Potential (V)**	**Polarization Resistance, R_p (Ω)**	**Cathodic Tafel Slope, B_c (V/dec)**	**Anodic Tafel Slope, B_c (V/dec)**
A	1.082	9.97E-05	9.97E-05	−0.589	257.70	−6.431	5.106
B1	2.353	2.17E-04	2.17E-04	−0.604	137.40	−4.932	2.998
B2	2.128	1.96E-04	1.96E-04	−0.594	563.20	−7.216	9.040
C1	3.665	3.38E-04	3.38E-04	−0.607	248.48	−6.558	11.233
C2	3.170	2.92E-04	2.92E-04	−0.605	180.10	−7.278	13.660

−0.627 V being the least electronegative. A gradual but progressive increase in OCP (sample B1) continues till the end of the exposure hours at −0.607 V (3200 s). Despite their more electronegative OCP values at 250 s, sample A and C1 displayed significant increase in OCP till 3200 s at −0.583 V and −0.600 V (sample A and C1). This shows that 1070AL (sample A) is more resistant to corrosion in the presence of SO_4^{2-} anions, though sample B1 and C1 achieve superior thermodynamic stability at 1600 s and 1900 s (−0.607 V −0.608 V) respectively.

OCP plots in Fig. 2(b) significantly contrast the plots in Fig. 2(a). The OCP values [Fig. 2(b)] initiated at comparatively higher electronegative potentials of −0.944 V, −1.006 V and −1.003 V at 0 s to values of −0.688 V, −0.772 V and −0.771 V at 250 s. The potential increase is due to formation of the protective aluminum oxide in the presence of Cl^- anion attack. However, the potentials are relatively lower than values obtained in Fig. 2(a). While the OCP plot of sample A and C1 after 250 s are at significantly higher potentials than the OCP plot for B1, potential transients are visible due to active passive electrochemical behavior of the protective oxide. The Cl^- anions being far smaller than SO_4^{2-} anions are capable of penetrating the oxide to initiate localized corrosion on alloy surface resulting in unstable passivation. This is quite visible at 1850 s (sample C1) and 2150 s (sample C1) where a sharp decrease in potential was observed. At 1850 s, a sharp increase in potential was also observed for sample A from −0.711 V to −0.674 V due to passivation of the alloy surface. The passive film formed on sample A tends to be more resilient. Comparison of Fig. 2(a) and (b) shows sample A (100% aluminum) is the most corrosion resistant followed by sample C1. Sample B1 consisting of 500 nm Al_2O_3 composites in the aluminum matrix has the highest tendency to corrosion but yet is the most thermodynamically stable. In Fig. 2(b) potential transients are completely absent from sample B1 OCP plots. In the presence of Cl^- and SO_4^{2-} anions [Fig. 2(c)], the OCP plots of sample A and B1 are the least electronegative followed by sample C1 by a small margin at 3200 s due to decrease in difference between the OCP values of sample C1, and sample A and B1. Potential transients dominate the OCP behavior with respect to exposure time due to the combined debilitating action of Cl^- and SO_4^{2-}. The samples in the combined sulphate/chloride solution are significantly thermodynamically unstable.

Optical microscopic image analysis

Morphological representations of 1070AL (sample A) and 1070AL/Al_2O_3 (sample B1 and C1) matrix composites (mag. ×40 and ×100) are shown from Figs. 3(a)–6(c). Fig. 3(a) and (b) shows the morphology of 1070AL and 1070AL/Al_2O_3 before corrosion, while Fig. 4(a)–(c) shows the morphology of 1070AL after corrosion in 0.1 M H_2SO_4, 1.78% NaCl and 0.1 M H_2SO_4/1.78% NaCl solutions respectively. Mild deterioration of 1070AL morphology occurred in 0.1 M H_2SO_4 solution [Fig. 4(a)] due to the action of SO_4^{2-} anions. This is represented as significant decrease of the anodic portion of the polarization plot [Fig. 1(a)] due to gradual deterioration of the surface properties of the metal alloy as earlier mentioned. The deterioration from optical microscopy is quite negligible as the surface appears to be slightly etched. In Fig. 4(b), while most of the surface area appears resistant to corrosion, corrosion pits are clearly visible due to localized corrosion reactions of Cl^- anions with the metal surface resulting in a pitted surface at specific sites on the metal, most especially at areas with flaws, inclusions and discontinuity of the passive film. Pit formation is basically due to adsorption and chemical interaction of Cl^- anions at these flaws in the surface oxide film [11]. Severe morphological deterioration occurred on 1070AL in Fig. 4(c) due to the combined action of SO_4^{2-} and Cl^- anions. Similar observation occurred for 1070AL/Al_2O_3 samples (sample B1 and C1) in similar solutions [Figs. 5(c) and 6(c)]; though the degree of deterioration in Fig. 5(c) is lower than Fig. 4(c). Observation of Fig. 5(b) shows the occurrence of intergranular corrosion or possibly localized corrosion resulting from breakages along cracks on the protective oxide. The difference between Fig. 4(b) and 5(b) is as a result of differences in the interfacial properties of the protective oxide resulting from changes in the metallurgy of the aluminum substrate due to the addition of Al_2O_3 nano-particles. This results in interfacial defects due

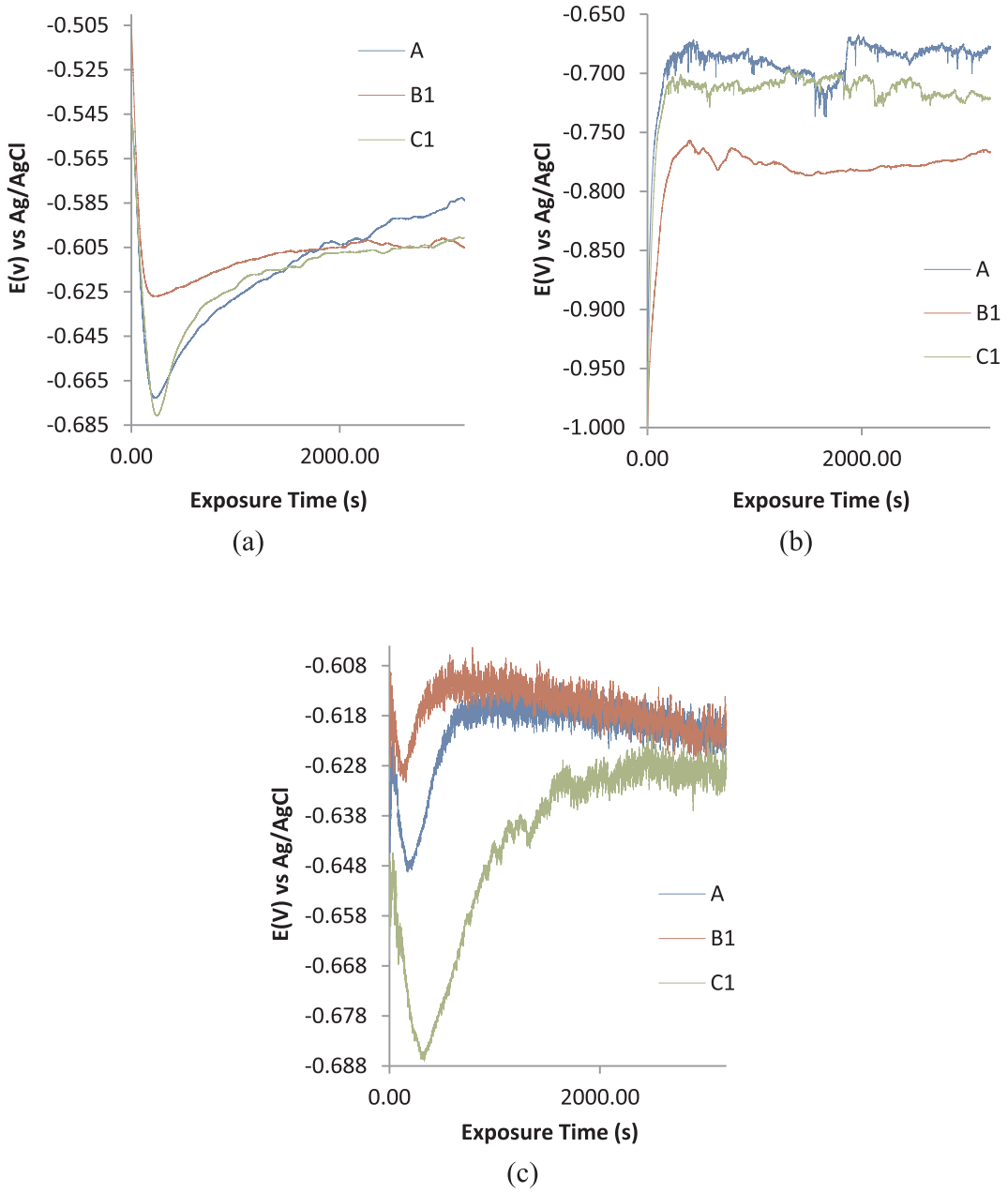

Fig. 2. Variation of OCP values against exposure time (a) 0.1 M H_2SO_4, (b) 1.78% NaCl and (c) 0.1 M H_2SO_4/1.78% NaCl solution.

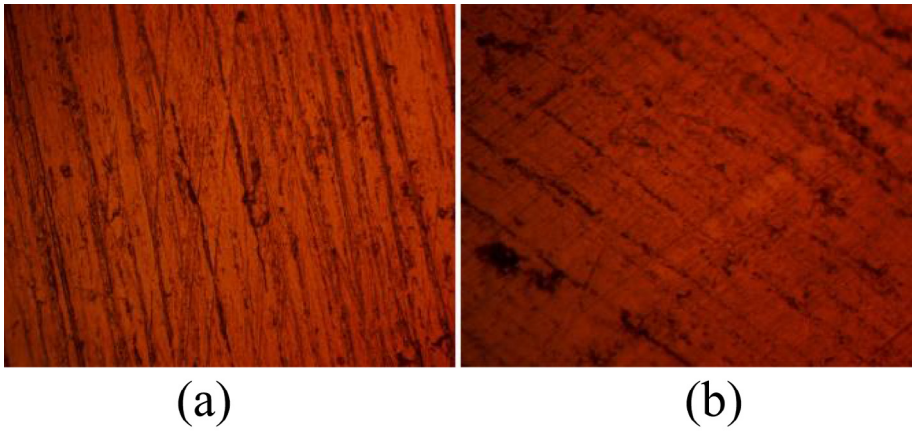

Fig. 3. Optical morphology of (a) 1070AL (sample A) and (b) 1070AL/Al_2O_3 before corrosion.

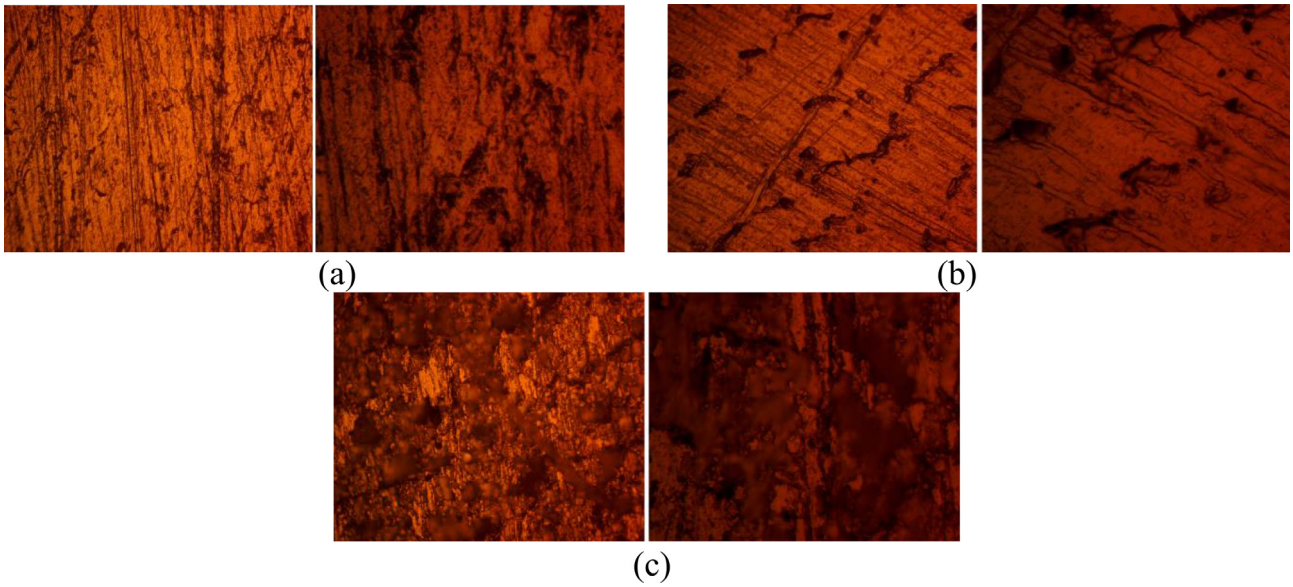

Fig. 4. Optical morphology of (a) sample A, (b) sample B1 and (c) sample C1 after corrosion in 0.1 M H_2SO_4 solution.

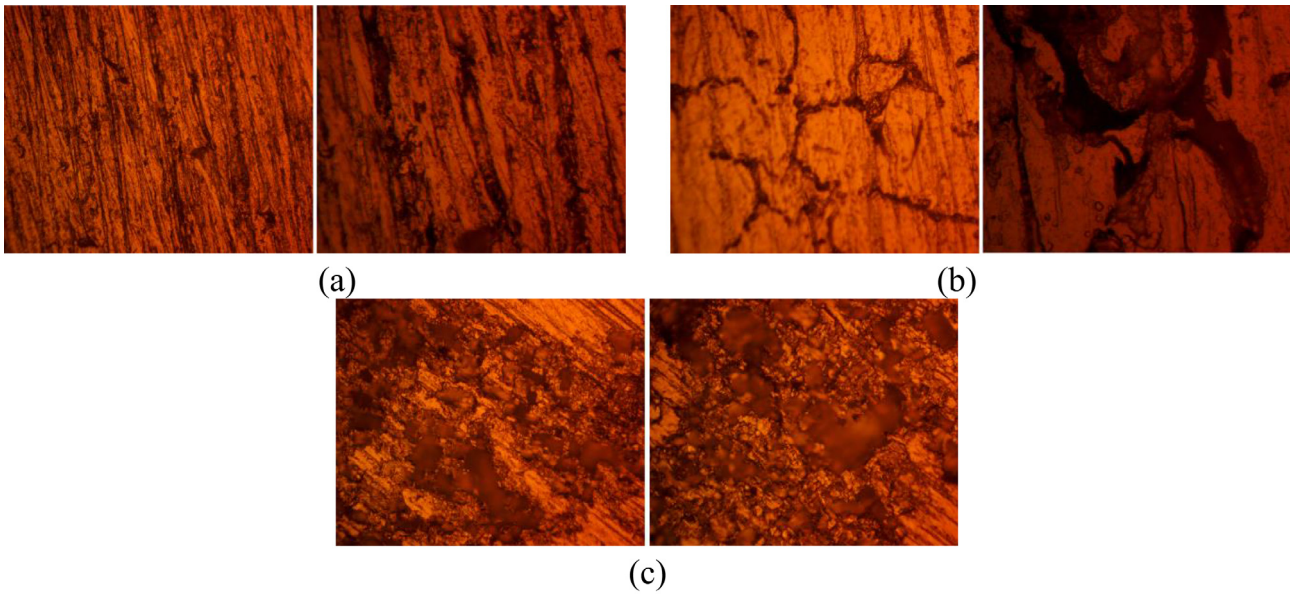

Fig. 5. Optical morphology of (a) sample A, (b) sample B1 and (c) sample C1 after corrosion in 1.78% NaCl solution.

to weak cohesion between Al_2O_3 and 1070AL matrix, causing the local chemistry at the defect sites to prevent passivation. 1070AL [Fig. 4(b)] without the presence of composites within its matrix is has a continuous protective oxide with minimal impurities hence the pitted morphology. 1070AL/Al_2O_3 [Fig. 5(b)] with 500 nm Al_2O_3 at 5% content within 1070AL matrix is most likely exposed to galvanic corrosion due to changes in the metallurgical structure of 1070AL as earlier mentioned and the presence of Al_2O_3 would have caused discontinuities in the protective oxide weakening the film and hence cause the localized corrosion reactions observed. Fig. 6(b) showed the presence of corrosion pits in contrast to Fig. 5(b). 1070AL/Al_2O_3 [sample C1, Fig. 6(b)] at 80 nm and 5% content displayed slightly similar morphological characteristics to 1070AL [sample A, Fig. 4(b)] in 0.1 M H_2SO_4 solutions. This observation is confirmed from the generally similar corrosion rate results in Table 3.

Conclusion

Aluminum alumina matrix composites at 80 nm particle size exhibited excellent corrosion resistance compared to the monolithic metal in 0.1 M H_2SO_4 and 1.78% NaCl solution while the matrix composites at 500 nm was the most corrosion resistant among the composites in 0.1 M H_2SO_4/1.78% NaCl solutions from potentiodynamic polarization and optical microscopic studies. In NaCl solution passivation behavior was observed due to formation of the protective oxide. Optical microscopy showed the presence of corrosion pits and intergranular cracks however

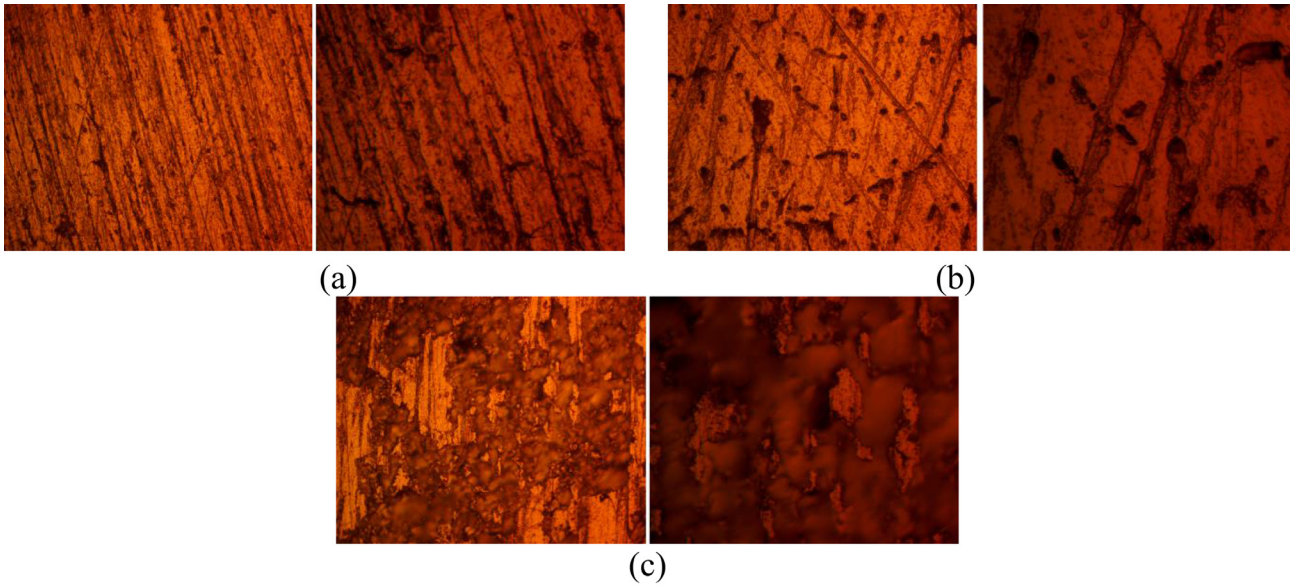

Fig. 6. Optical morphology of (a) sample A, (b) sample B1 and (c) sample C1 after corrosion in 0.1 M H_2SO_4/1.78% NaCl solution.

the presence of alumina did not decrease the corrosion resistance of the matrix composite.

Acknowledgement

The author is grateful to Covenant University for the sponsorship of the research and provision of research facilities.

Conflict of interest

The authors declare no conflict of interest.

Appendix A. Supplementary data

Supplementary data associated with this article can be found, in the online version, at https://doi.org/10.1016/j.rinp.2018.07.025.

References

[1] Schacht M, Boukis N, Dinjus E. Corrosion of alumina ceramics in acidic aqueous solutions at high temperatures and pressures. J Mater Sci 2000;35(24):6251–8. https://doi.org/10.1023/A:1026714218.
[2] Ćurković L, Jelača MF, Kurajica S. Corrosion behavior of alumina ceramics in aqueous HCl and H_2SO_4 solutions. Corros Sci 2008;50(3):872–8.
[3] Mikeska KR, Bennison SJ. Corrosion of alumina in aqueous hydrofluoric acid. J Am Ceram Soc 1999;82(12):3561–6.
[4] Lazar A-M, Yespica WP, Marcelin S, Pébère N, Samélor D, et al. Corrosion protection of 304L stainless steel by chemical vapour deposited alumina coatings. Compos. Elsevier 2014;81:125–31. https://doi.org/10.1016/j.corsci.2013.12.012.
[5] Alaneme K, Bodunrin M. Corrosion behavior of alumina reinforced aluminium (6063) metal matrix composites. J Miner Metall Mater Eng 2011;10(12):1153–65. https://doi.org/10.4236/jmmce.2011.1012088.
[6] Parvina N, Rahimian N. The characteristics of alumina particle reinforced pure Al matrix composite. Acta Phys Pol A 2012;121(1):108–10.
[7] Loto RT, Adeleke A. Corrosion of aluminum alloy metal matrix composites in neutral chloride solutions. J Fail Anal Prev 2016;16(5):874–85.
[8] Loto RT, Babalola P. Corrosion polarization behavior and microstructural analysis of AA1070 aluminium silicon carbide matrix composites in acid chloride concentrations. Cogent Eng 2017;4:1422229. https://doi.org/10.1080/23311916.2017.1422229.
[9] Loto RT, Babalola P. Analysis of SiC grain size variation and NaCl concentration on the corrosion susceptibility of AA1070 aluminium matrix composites. Cogent Eng 2017;5:1473002. https://doi.org/10.1080/23311916.2018.1473002.
[10] Hihara LH. Corrosion of metal-matrix composites. ASM Handbook Vol. 13B. Materials Park, OH: ASM International; 2005. p. 526–42.
[11] Aylor DM, Taylor D. Corrosion of metal matrix composites. ASM Handbook Vol. 13. Materials Park, OH: ASM International; 1999. p. 859–63.
[12] Rahimian M, Parvin N, Ehsani N. The effect of production parameters on microstructure and wear resistance of powder metallurgy Al-Al_2O_3 composite. Mater Des 2011;32:1031–8. https://doi.org/10.1016/j.matdes.2010.07.016.
[13] Kok M, Ozdin K. Wear resistance of aluminum alloy and its composites reinforced by Al_2O_3 particles. J Mater Processes Technol 2007;183(2–3):301–9. https://doi.org/10.1016/j.jmatprotec.2006.10.021.
[14] Foley RT. Localized corrosion of aluminum alloys—a review. Corrosion 1986;42(5):277–88. https://doi.org/10.5006/1.3584905.